International Refrigeration and Air Conditioning
Conference

School of Mechanical Engineering

2021

Development of Novel Experimental Infrastructure for Collecting High-Fidelity Experimental Data for Refrigerant to Air Heat Exchangers

Saad Saleem
Oklahoma State University, Mechanical & Aerospace Engineering, Stillwater, OK 74075, USA,
saad.saleem@okstate.edu

Omer Sarfraz

Craig R. Bradshaw

Christian K. Bach

Follow this and additional works at: https://docs.lib.purdue.edu/iracc

Saleem, Saad; Sarfraz, Omer; Bradshaw, Craig R.; and Bach, Christian K., "Development of Novel Experimental Infrastructure for Collecting High-Fidelity Experimental Data for Refrigerant to Air Heat Exchangers" (2021). *International Refrigeration and Air Conditioning Conference.* Paper 2113.
https://docs.lib.purdue.edu/iracc/2113

Development of Novel Experimental Infrastructure for Collection of High-Fidelity Experimental Data of Refrigerant to Air Heat Exchangers

Saad SALEEM[(a)]*, Omer SARFRAZ[(b)], Craig R. BRADSHAW[(c)], Christian K. BACH[(d)]

[(a) (c) (d)] Oklahoma State University, Mechanical & Aerospace Engineering,
Stillwater, OK 74075, USA

[(b)] Johnson Controls Inc., York, PA 17403, USA

[(a)] saad.saleem@okstate.edu, [(b)] omer.sarfraz@jci.com, [(c)] craig.bradshaw@okstate.edu,[(d)] cbach@okstate.edu

ABSTRACT

Manufactures of fin-and-tube heat exchangers often employ predictive modelling tools in order to reduce development cost and time. These tools require high-fidelity experimental data to validate the accuracy of their predictions. To that end, this paper presents the design and development of a custom-designed pumped refrigerant loop to collect high-fidelity experimental data for fin-and-tube heat exchangers in three operating modes: (1) single-phase refrigerant, (2) evaporator, and (3) condenser mode. It is combined with a small-scale wind tunnel installed in a psychrometric chamber facility for the purpose of validating the recently developed discretized fin-and-tube heat exchanger models (Sarfraz *et al.*, 2019a and 2019b). The pumped refrigerant loop is able to precisely control desired refrigerant test conditions, flowrate to each individual heat exchanger circuit, and has been sized in order to test heat exchanger coils up to a capacity of 5 tons (17.5 kW). A preliminary test plan and uncertainty analysis is presented for the first heat exchanger coil to be tested. The uncertainty analysis showed that the experiment will have the capability of measuring overall coil capacity within ±2%. A design of experiments is also presented, which suggests that 9 tests per coil is an adequate number for minimizing experimental effort. A preliminary experiment was performed which showed that the average air and refrigerant side capacities match to within 1.1% of each other. This provides evidence that the experimental setup has the capability to far exceed the 5% threshold set by ASHRAE Standard 33 (2016).

1. INTRODUCTION AND MOTIVATION

For air-to-refrigerant applications in residential and light-commercial air-conditioning, heating, ventilation, and refrigeration (HVAC&R) systems, fin-and-tube heat exchangers are widely used because of their low cost and ease of manufacturing. Manufacturers of these heat exchangers can leverage numerical models to reduce experimental iterations while developing new products. Models with high-fidelity require validation data that has equally high-fidelity.

Extensive experimental investigation of fin-and-tube heat exchangers has been carried out over the years to study the effects of various parameters, with a wide variety of test setup configurations and refrigerants. Liang *et al.*, (2001) developed a discretized heat exchanger model to investigate the performance of fin-and-tube evaporator coils with complex refrigerant circuitry. The refrigerant conditioning loop comprised of a vapor compression cycle in which a manual expansion valve (EXV) controlled refrigerant flow rate, with a variable speed compressor used for setting refrigerant side capacity during evaporator operation. Lee *et al.* (2003) also developed a discretized heat exchanger model whose experimental validation was performed by conducting several tests on two different multi-circuit evaporators. The setup was comprised of a vapor compression system, along with a chilled water loop to control refrigerant sub-cooling at the evaporator inlet. The experimental setup could be used only for testing evaporator coils. The refrigerant loop had incorporated capillary tubes, downstream of the distributor, in order to assign the same refrigerant flow to each individual circuit. Domanski *et al.* (2007) experimentally assessed how tube-to-tube heat transfer occurring by conduction through fins affected the performance of fin-and-tube evaporators at varying refrigerant exit superheats. The experimental setup consisted of a vapor compression loop as the test rig, a chilled water loop and an air flow loop. The vapor compression loop had a variable speed compressor, water cooled shell-

and-tube condenser, sub-cooler and one EXV per circuit. A pressure regulating valve downstream of the evaporator coil was used for controlling evaporator exit pressure, while the EXVs were used for controlling exit superheat of each circuit. In comparison to the previously mentioned setups, this facility had an additional feature of controlling refrigerant flow rate to each independent circuit. Wang *et al.* (2016) presented experimental testing and numerical modelling to evaluate how refrigerant side maldistribution in a multi-circuit evaporator is affected by various geometric factors. The test setup, using R410A, comprised of a vapor compression loop with some additional components including an extra compressor and sub-condenser cooling loop, for testing cooling coils of a capacity of 3 to 40 kW. Castro *et al.* (2005) did experimental testing and numerical modelling of a reversible air-to-water heat pump, using R290 as refrigerant, to find the best fin-and-tube heat exchanger coil configuration. The heat pump was comprised of a fin-and-tube heat exchanger, scroll compressor, brazed plate heat exchanger (BPHE) and a TXV. The water-side of the heat pump unit comprised of a pumped hydraulic loop connected to the BPHE. Two evaporators with different circuit lengths and number of circuits were tested.

Even though a lot of work has been done to investigate fin-and-tube heat exchanger performance, the literature search did not reveal many experimental setup configurations that tested both, evaporator (cooling) as well as condenser (heating) coils. Additionally, majority of the setups that tested multi circuit coils did not have the capability to assign varying refrigerant flow rate to each individual circuit, so as to test the coils at part load. Finally, no experimental facility was found that could do all the above while also providing the flexibility to test single-phase refrigerant.

This paper outlines the design and development of a custom pumped refrigerant loop coupled with a small-scale wind tunnel and an existing psychrometric chamber facility that will achieve all aforementioned features. This will allow the acquisition of high-fidelity data to validate a discretized heat exchanger numerical model developed by Sarfraz *et al.* (2019a) The pumped refrigerant loop allows precise maintenance of the desired test conditions and flowrate of refrigerant and has been sized to test heat exchanger coils up to a capacity of five tons in cooling and heating mode. In addition, the pumped refrigerant loop has the ability to test both, evaporator as well as condenser coils, simply by using a combination of different valves in open and closed positions.

2. HEAT EXCHANGER TESTING FACILITY

The experimental apparatus for evaluating the performance of fin-and-tube heat exchanger test coils combines an airside ductwork with an ASHRAE code tester installed in a psychrometric chamber facility with a pumped refrigerant loop, as shown in Figure 1. The articles focuses on the refrigerant loop; details of the psychrometric chamber facility can be found in Lifferth (2009) and Aslan (2010), while the airside ductwork is described in Lee *et al.*, (2018 and 2019).

2.1 Pumped refrigerant loop design and operation
Tests were conducted in a wind tunnel that allows the flow of conditioned air through the test heat exchanger coils. A schematic of the wind tunnel is shown in Figure 1. The wind tunnel has been designed for the first test coil, having face area dimensions of length 44.5 cm (17.5 inches) and height of 40.64 cm (16 inches). It is housed in the outdoor room of a psychrometric chamber facility, whose temperature and humidity control ranges (Cremaschi & Lee, 2008) are suitable for the desired test conditions of this study. The outdoor room`s flow measurement bay (code tester) generates the required air flow for coil testing and also measures the air flow rate. Air circulation in the chamber can be seen in Figure 1 where the coils tested for this study will be installed in the "setup" section upstream of the code tester. The air circulation process is detailed in Lee *et al.*, (2018).

The pumped refrigerant loop has been designed to operate with R410A and sized for testing heat exchanger coils up to a capacity of 5 tons (17.5 kW). It provides control of: (1) refrigerant mass flow rate in the loop, (2) saturated suction temperature (SST) of refrigerant at inlet to heat exchanger, and (3) superheat (SH) of refrigerant at heat exchanger outlet (for evaporator testing) or subcooling (SC) (for condenser testing).
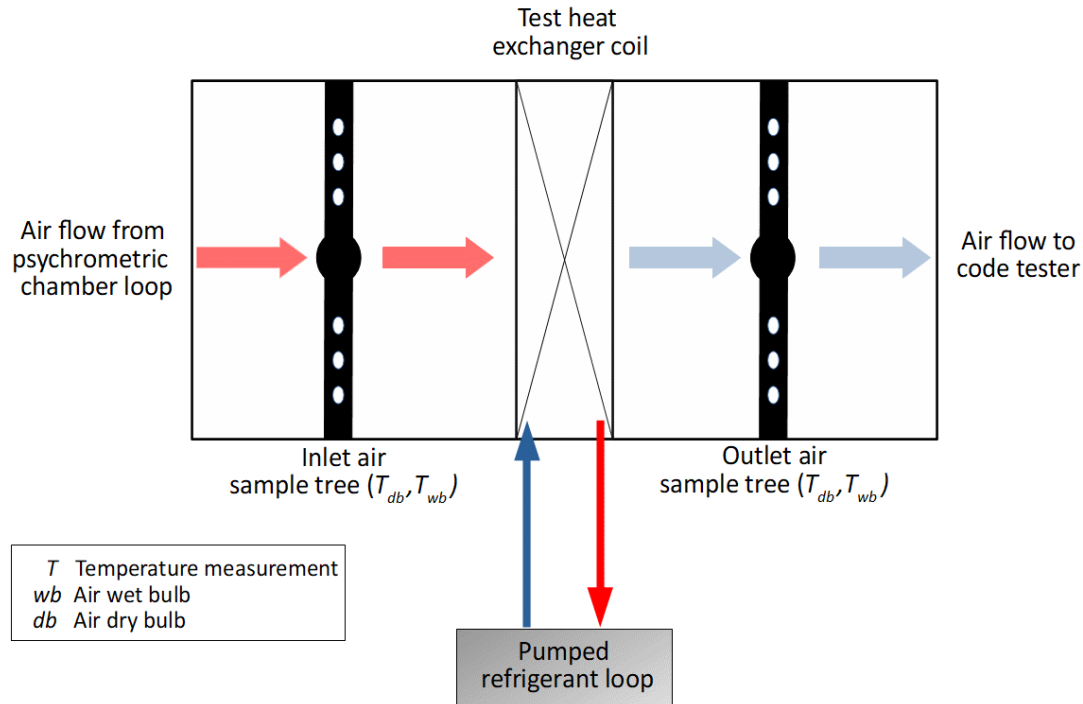
Figure 1: Schematic diagram of the small-scale wind tunnel

Figure 2 shows the operation of the pumped refrigerant loop operating in evaporator mode. Refrigerant evaporates in the coil under test from points 1 to 2 and enters the heat rejection units at point 3, which are modified water-to-water heat pumps having a combined nominal cooling capacity of 21.1 kW (6 tons), where refrigerant vapor is condensed. After exiting the 2nd heat rejection unit at point 5, the subcooled refrigerant passes through the refrigerant pump to point 6. Refrigerant exiting the pump goes through a filter drier and is then pumped through a water-to-refrigerant BPHE (points 7 to 8) to set the refrigerant SST. Finally, the refrigerant is now at the desired state and enters the test heat exchanger at point 1 via the EXVs, which can expand the refrigerant down to the required inlet two-phase quality. The entire refrigerant circulation process mentioned above repeats during the operation of the refrigerant conditioning loop. A sight glass installed at the suction to the refrigerant pump allows to monitor flow conditions. Moreover, a bladder accumulator in the loop is also present and is used to set refrigerant pressure during single-phase refrigerant tests.

2.2 Pumped refrigerant loop controls scheme

LabVIEW was used to implement a control scheme of the pumped refrigerant loop and data collection from the instrumentation attached to it. Refrigerant mass flow rate is controlled by adjusting the frequency output of the variable frequency drive (VFD) attached to the refrigerant pump. The refrigerant SST is controlled via adjustment of the input power to the water heater by means of a Silicon-Controlled Rectifier (SCR). Additionally, a series of EXV's are installed at the inlet to the tested coil (state 1) which are adjusted automatically to control superheat at heat exchanger exit when operated in evaporator mode, and the subcooling when operated in condenser mode.

3. PRELIMINARY TEST PLAN

A preliminary test plan is formulated for the first coil that will be tested in the refrigerant conditioning loop. This coil, having sine-wave fins, is comprised of 4 circuits with 12 tubes in each circuit and 48 tubes in total as shown in Figure 3, which presents a photograph and circuiting schematic of this coil. The objective of this test plan is to minimize the number of data points required to explore each test variable, called design factors, in order to test the highest number of unique test variables. To accomplish this, a formalized method called full factorial design is used.
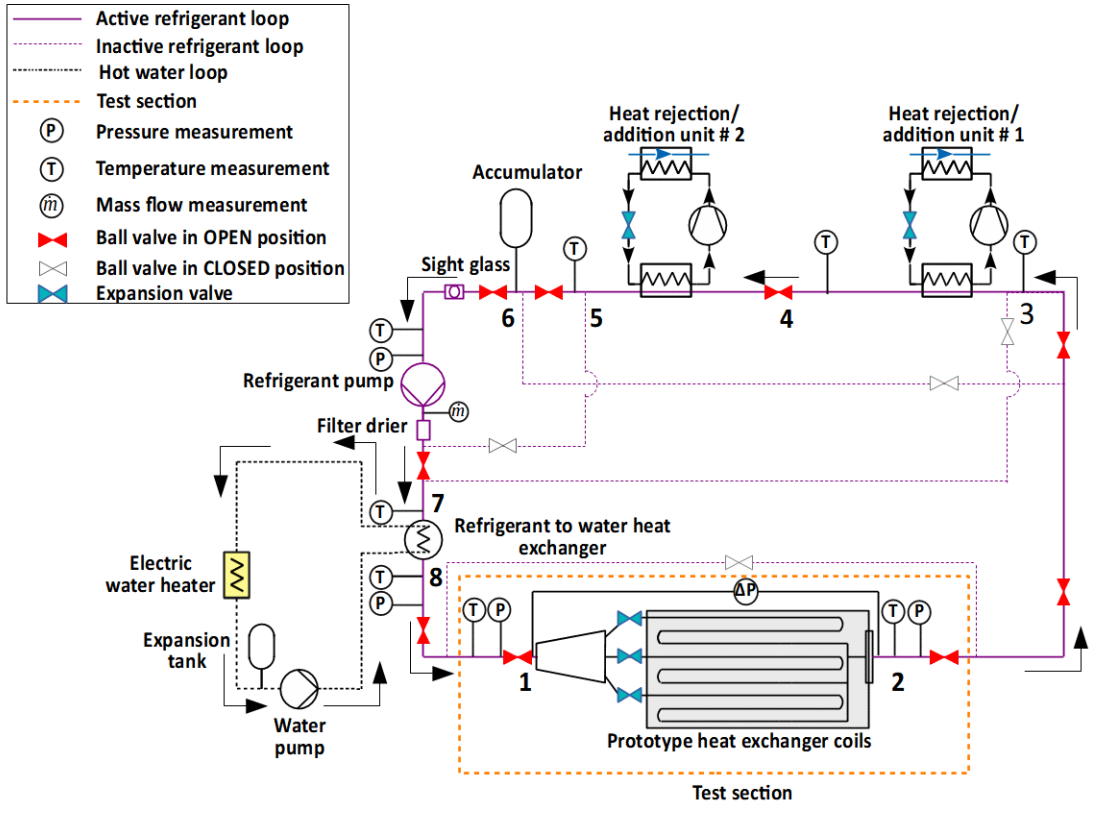
Figure 2: Schematic diagram of pumped refrigerant loop (operating in evaporator mode) and trim heating loop

a) Photograph of test coil
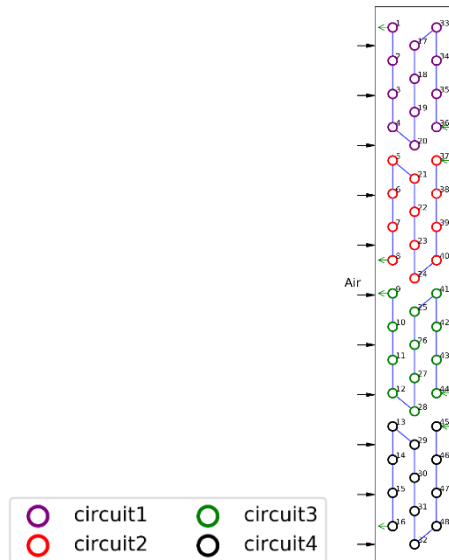
b) Circuit schematic of test coil

Figure 3: First test coil

The preliminary test plan is based on the full factorial design of experiments with the control run (center point), presented by Myers & Montgomery (1995), in which the total number of required experiments is estimated by $2^n + 1$, where n is the number of design factors. In this experiment, heat exchanger coil capacity is the critical outcome and the design factors are selected based on past experience of the authors and collaborators with heat exchanger testing,

namely: (1) SST of refrigerant, (2) SH of refrigerant, and (3) air velocity at coil face $(v_{a,i})$. The range of the design factors selected for testing the first coil in evaporator mode are listed in Table 1.

Table 1: Range of design factors

Factors	Minimum value ($-$)	Maximum value ($+$)
Saturated suction temperature (*SST*)	7.22°C (45°F)	12.78°C (55°F)
Air inlet velocity ($v_{a,i}$)	1 m/s (200 fpm)	2 m/s (400 fpm)
Test superheat (*SH*)	5.56°C (10°F)	12.22°C (22°F)

Both the refrigerant enthalpy at the coil inlet and the air inlet dry and wet bulb temperatures will be fixed during the exploration of the design space. These 9 test points in the design space will be repeated for various inlet air conditions and coil models of operation including wet and dry evaporator tests and condenser tests. The air, dry, wet bulb and dew point temperatures to test the coil in evaporator and condenser modes are given in Table 2.

Table 2: Air temperatures for tests in evaporator and condenser mode

Mode	Dry bulb temperature	Wet bulb temperature	Dew point temperature
Evaporator dry	26.67°C (80°F)	14.44°C (58°F)	4.44°C (40°F)
Evaporator wet	26.67°C (80°F)	19.44°C (67 °F)	15.56°C (60°F)
Condenser	26.67°C (95°F)	23.89°C (75°F)	19.17°C (66.5°F)

Table 3 lists the test conditions for the dry evaporator test.

Table 3: Conditions for the dry evaporator test

Air dry bulb temperature	Air wet bulb temperature	Liquid line temperature	Saturated suction temperature	Air inlet velocity	Superheat
26.67°C (80°F)	14.44°C (58°F)	35°C (95°F)	7.22°C (45°F)	1 m/s (200 fpm)	5.56°C (10°F)
			12.78°C (55°F)		
			7.22°C (45°F)	2 m/s (400 fpm)	
			12.78°C (55°F)		
			7.22°C (45°F)	1 m/s (200 fpm)	12.22°C (22°F)
			12.78°C (55°F)		
			7.22°C (45°F)	2 m/s (400 fpm)	
			12.78°C (55°F)		
			10°C (50°F)	1.5 m/s (400 fpm)	8.89°C (16°F)

Figure 4 (a) shows the points for full factorial design. After executing the initial test matrix, locations of the critical design points will be revealed. These are the points that produce a considerable change in coil capacity and will be used as a litmus test to determine which of the parameters are most critical and encourage additional testing between those points to add additional test fidelity. As an example, 2 critical design points out of 9 design points are shown in Figure 4 (b). Once the critical design points will be located, further design points in the vicinity of the critical design points will be explored as shown in Figure 4 (c).

4. UNCERTAINTY ANALYSIS

An uncertainty analysis is performed for the air and refrigerant side based on the standard uncertainty of the selected instrumentation.
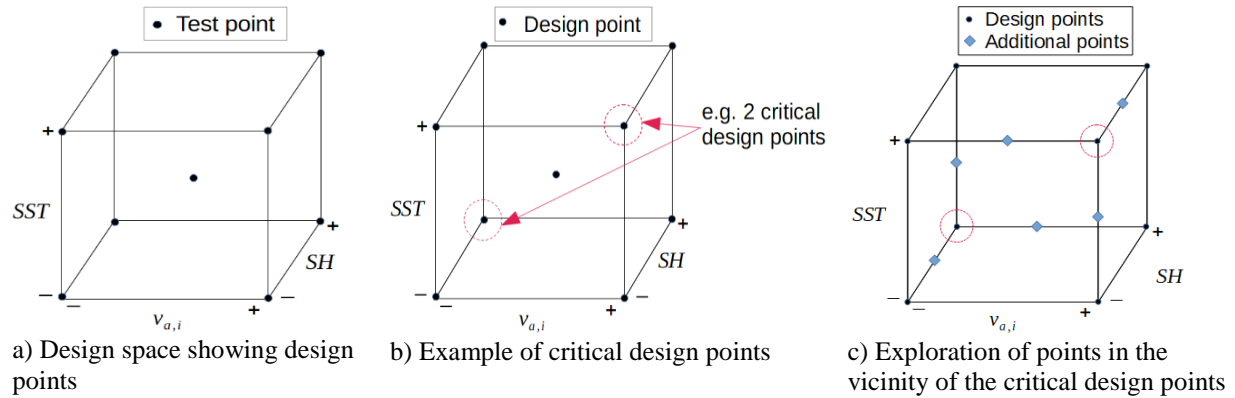
a) Design space showing design points   b) Example of critical design points   c) Exploration of points in the vicinity of the critical design points

Figure 4: Illustration of the full factorial design of experiments for developing the test matrix for heat exchanger testing

5.1 Airside uncertainty

The overall airside capacity, $\dot{Q}_{air}$ is given by Equation (1).

$$\dot{Q}_{air} = \dot{m}_{air} \cdot \left(h_{a,bht} - h_{a,aht} \right), \tag{1}$$

The uncertainty of each term will be individually explored in the following section starting with the air mass flow rate. The volumetric air flow rate is calculated using a nozzle box containing different set of nozzles to cover a wide range of flow rates. To calculate air mass flow rate, measurements of differential pressure across the nozzle set, the air temperature and pressure at the nozzle inlet, and the nozzle diameter are required as inputs to the equations given in ASHRAE Standard 37 (2009). The type, measurement range, and the accuracy of instruments used to measure these parameters in this facility are listed in Table 4.

Table 4: Information on instrumentation for parameters needed for airflow calculation

Parameter	Instrument		
	Type	Range	Accuracy
Differential pressure across nozzle	Differential pressure transducer	0-747 Pa	±0.25% full scale
Nozzle diameter (ND)	Not Applicable	0-6 in	0.002·ND[1]
Temperature (dry and wet bulb) at nozzle inlet	RTD[2]	5-75°C	±0.06°C[3]
Pressure at nozzle inlet	Pressure transducer	-374 to 374 Pa	±0.25% full scale
Barometer	Pressure transducer	80-110 kPa	±0.03 kPa

The uncertainty propagation in flow rate due to the uncertainties of the parameters in Table 4 is calculated using Section 7 of the ASME PTC 19.1 (2013). It states that for the result R and its parameters $(X_1, X_2, \ldots, X_i, \ldots, X_N)$, the sensitivity coefficient θ_i for parameter X_i can be found using partial differentials as: $\theta_i = \frac{\partial R}{\partial X_i}$, where partial derivative can be evaluated analytically or numerically using finite difference approach. The uncertainty in the result, δR if the uncertainty in the parameters $(X_1, X_2, \ldots, X_N)$ are $\delta X_1, \delta X_2, \ldots, \delta X_N$ can be found using equation 2.

$$\delta R = \sqrt{(\theta_1 \cdot \delta X_1)^2 + (\theta_2 \cdot \delta X_2)^2 + \cdots + (\theta_N \cdot \delta X_N)^2} \tag{2}$$

---

[1] *Nozzle Diameter*
[2] *Resistance Temperature Detector*
[3] *Calibrated to a reference thermometer with ±0.06°C rated accuracy*

The coil inlet velocity will be controlled to vary from 1 to 2 m/s (200 to 400 fpm) as described in the test plan section. The first coil to be tested in this environment has a face area of 0.18 m² (1.94 ft²), resulting in an airflow rate of 0.19 to 0.38 m³/s (400 to 800 cfm). The selected nozzles have a pressure drop of 156 Pa (0.6 in WC) at the maximum airflow rate of 0.19 m³/s (800 cfm).

Figure 5 shows the uncertainty propagation results of airflow rate due to the uncertainties of its parameters. It shows how the individual contribution of various parameters, namely the differential pressure measurement across the nozzle (ΔP), nozzle diameter (ND), air side dry bulb temperature, $T_{a,db}$, wet bulb temperature, $T_{a,wb}$ and, pressure at nozzle inlet (P_a) vary with increasing air flow rate.
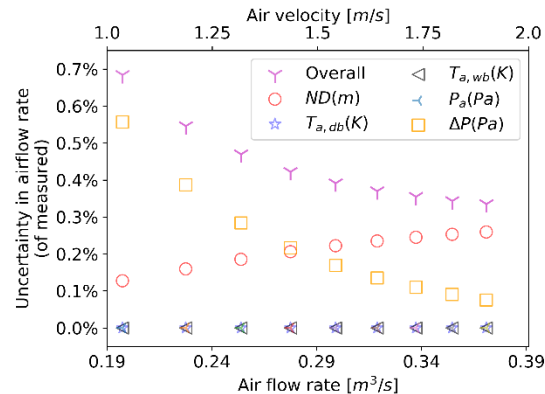
Figure 5: Effect of airflow rate on uncertainty contributors (using 0.1016 m (4 in) and 3 in (0.0762 m) diameter nozzles)

The outlet and inlet air enthalpies are also required for air capacity calculation and are calculated by measuring air dry and wet bulb temperatures. To achieve this, there are two RTDs at the coil inlet and two RTDs at the coil exit with each calibrated to a reference thermometer with ±0.06 °C rated accuracy and measurement range of 5 - 75 °C.

The individual uncertainties calculated previously can then be incorporated into a total propagated uncertainty of the coil capacity. To accomplish this, the nominal capacity of the initial test coil is used (5.5 kW) to first estimate the outlet air conditions from the coil for a given set of inlet conditions for the wet evaporator test (see Table 3) at an air flow rate of air flow rate of 0.38m³/s (800 cfm). The air outlet conditions are then fixed and the airflow rate is varied from 0.19 to 0.38 m³/s (400 to 800 cfm) to obtain the airside capacity as a function of airflow rate.

Figure 6 shows the result of this uncertainty propagation analysis in the airside capacity due to uncertainty in its various parameters. The overall uncertainty in the air side capacity is within 2.0% of the measure value.
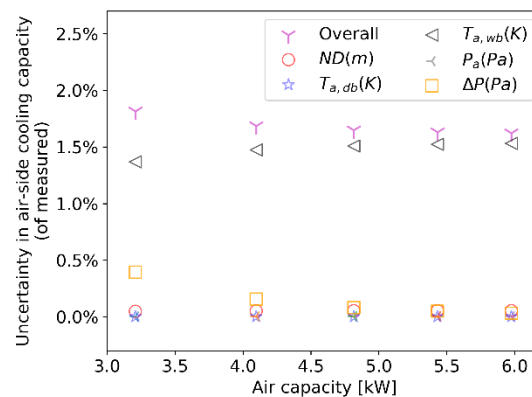
Figure 6: Effect of air-side cooling capacity on uncertainty contributors

5.2 Refrigerant side uncertainty

The refrigerant capacity is given by Equation (2).

$$\dot{Q}_{ref} = \dot{m}_r \cdot \left(h_{r,out} - h_{r,in}\right), \tag{3}$$

The refrigerant enthalpy is calculated by measuring its temperature and pressure. The type, measurement range, and accuracy of instruments used to measure the parameters for refrigerant capacity calculation are provided in Table 5.

Table 5: Instrumentation information for refrigerant capacity calculation

Parameter	Instrument		
	Type	Range	Accuracy
Refrigerant mass flow rate	Mass flow meter	0-1 kg/s	±0.05% of measured
Refrigerant temperature before and after coil	RTD	5-90°C	±0.06°C[1]
Refrigerant pressure before and after coil	Pressure transducer	0-500 psi	±0.42 psi[2]

Figure 7 shows the uncertainty propagation in the refrigerant capacity due to the individual uncertainty in its parameters. The overall relative uncertainty in the refrigerant capacity is within 0.2% of the measured value with refrigerant pressure contributing more than 44% to the overall uncertainty.
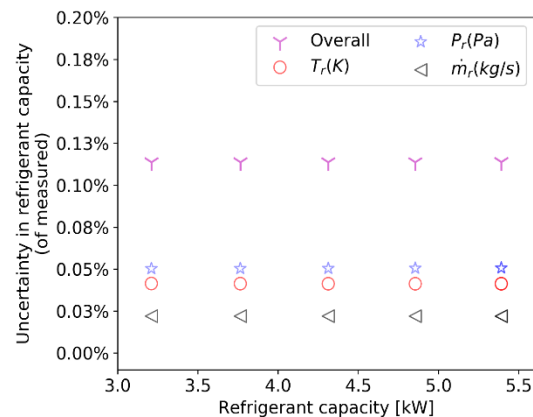
Figure 7: Relative uncertainty in refrigerant capacity due to different parameters

5.3 Preliminary Testing - Energy balance between air and refrigerant capacities

According to ASHRAE Standard 33 (2016), the capacities on the air and refrigerant side shall agree within 5% as the average of these capacities is the capacity of the coil. To verify that the experimental facility can conform to these capacity tolerance limits, a preliminary test was run, using single-phase refrigerant in evaporator (dry) mode. For the given test, the set points for SST and $\dot{m}_r$ were 10°C (50°F) and 0.33 kg/s (2,619 lbs. per hour) respectively. On the air side, the set points for $v_{a,i}$ and $T_{a,db}$ were 1 m/s (200 fpm) and 26.67°C (80°F) respectively. Data collection was initiated at a rate of 1 sample per seconds for a total of 15 minutes, once air and refrigerant side reached steady state and the capacities were within 5% of each other. Figure **8** shows the comparison of air and refrigerant side capacities for the preliminary test.

The refrigerant side capacity has a lower random uncertainty in comparison to the airside. Moreover, for the entire testing duration, air and refrigerant side capacities were within 1.1% of each other on average, thus exceeding the threshed hold limit set by ASHRAE 33 (2016).

---

[1] *Calibrated to a reference thermometer with ±0.06°C rated accuracy*

[2] *In-house calibrated, manufacturer rated accuracy is 0.13% full scale*

5. CONCLUSIONS

The paper presents the design and development of a custom designed pumped refrigerant loop to collect high-fidelity data for validating a segment-by-segment fin-and-tube heat exchanger model. A literature survey found that the designed pumped refrigerant loop is unique because it can test cooling (evaporator) as well as heating (condenser) coils in addition to single-phase refrigerant tests using the same test setup simply by changing valve positions in the refrigerant loop. The design and operation of this novel facility is presented which highlights its flexibility and features. Additionally, detailed operation is described for the loop in evaporator mode. A preliminary test plan is provided for the first coil that was tested in the experimental setup. The design of experiments method presented will be used to identify areas of critical sensitivity in need of additional experimental fidelity.
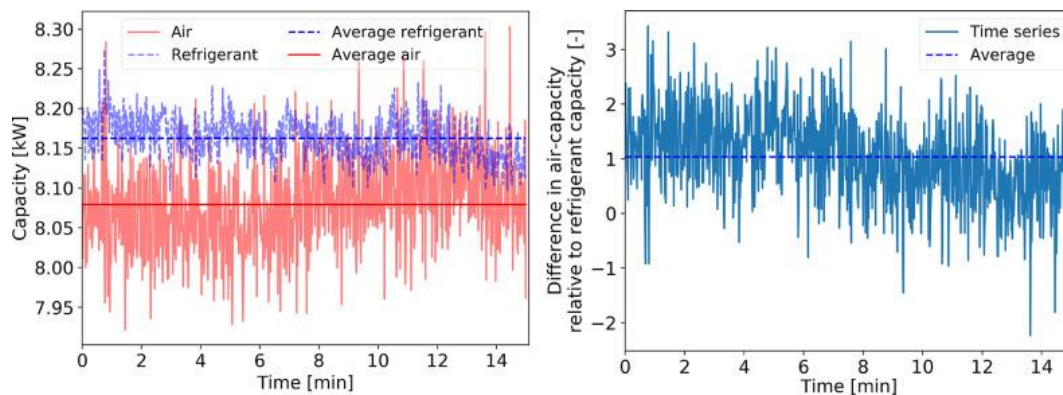
Figure 8: Energy balance on refrigerant and air side, (a) Refrigerant and air side capacities, (b) Percentage difference in air-capacity relative to the refrigerant capacity

Results of an uncertainty analysis are also presented in detail, which determine the uncertainty propagation in the air and refrigerant side capacity based on the standard uncertainty of the selected instrumentation. It was found that the relative uncertainty in the refrigerant capacity and airside capacity is within 0.2% and 2% respectively for all planned points in the initial test matrix. A preliminary experiment shows that the air and refrigerant side capacities were within 1.1% of each other, thus exceeding the 5% energy balance limit on refrigerant and airside as per ASHRAE Standard 33 (2016). A future publication will show how numerical models compare against high-fidelity experimental data obtained from the experimental facility.

NOMENCLATURE

BPHE	Brazed plate heat exchanger	SCR	Silicon-controlled rectifier
DAQ	Data acquisition system	SH	Superheating (K)
EXV	Expansion valve	SST	Saturated suction temperature (°C)
P	Pressure	T	Temperature
RTD	Resistance temperature detector	TXV	Thermostatic expansion valve
SC	Subcooling (K)	VFD	Variable frequency drive
$\dot{m}$	Mass flow (kg/s)	$\dot{Q}$	Heat transfer (W)
v	Velocity (m/s)	h	Enthalpy, J/kg-K

Subscript and symbols

a, air	air	*r, ref*	Refrigerant
aht	After heat exchanger	*bht*	Before heat exchanger

| *i, in* | Inlet | *o, out* | Outlet |
| Δ | Differential | | |

6. ACKNOWLEDGEMENTS

REFERENCES

American Society of Heating, Refrigerant and Air Conditioning Engineers, I. (2016a). *ASHRAE Standard 33 - Methods of testing for rating electrically driven unitary air conditioning and heat pump equipment*. Atlanta, USA.

American Society of Heating, Refrigerant and Air Conditioning Engineers, I. (2016b). *ASHRAE Standard 51-16 (ANSI/AMCA Standard 210-16. Laboratory Methods Of Testing Fans For Certified Aerodynamic Performance Rating*. Atlanta, USA.

ANSI/ASHRAE Standard 37-2009. (2009). *Methods of Testing for Rating Electrically Driven Unitary Air-Conditioning and Heat Pump Equipment*. Atlanta, USA: American Society of Heating, Refrigeration and Air-Conditioning Engineers.

Aslan, O. (2010). *Sensors, Instrumentation and Process Control System Design of the OSU Psychrometric Chamber*. Oklahoma State University.

ASME PTC 19.1 - 2013. (2013). Test uncertainty - Performance Test Codes. New York: American Society of Mechanical Engineers.

Castro, J. B., Urchueguía, J. F., Corberán, J. M., & Gonzálvez, J. (2005). Optimized design of a heat exchanger for an air-to-water reversible heat pump working with propane (R290) as refrigerant: Modelling analysis and experimental observations. *Applied Thermal Engineering*, *25*(14–15), 2450–2462. https://doi.org/10.1016/j.applthermaleng.2004.12.009

Cremaschi, L., & Lee, E. (2008). Design and heat transfer analysis of a new psychrometric environmental chamber for heat pump and refrigeration systems testing. *ASHRAE Transactions*, *114*(2), 619–631.

Domanski, P. A., Choi, J. M., & Payne, W. V. (2007). Longitudinal heat conduction in finned-tube evaporators. In *International Congress of Refrigeration*.

Lee, J. A., Bach, C. K., & Bradshaw, C. (2018). CFD Case Study : Heat Exchanger Inlet Air Velocity Distribution for Ducted Tests in a Psychrometric Chamber (ASHRAE RP-1785). In *International Refrigeration and Air Conditioning Conference at Purdue*. West Lafayette. Retrieved from https://docs.lib.purdue.edu/iracc/2068/

Lee, J., Kwon, Y. C., & Kim, M. H. (2003). An improved method for analyzing a fin and tube evaporator containing a zeotropic mixture refrigerant with air mal-distribution. *International Journal of Refrigeration*, *26*(6), 707–720. https://doi.org/10.1016/S0140-7007(03)00023-9

Liang, S. Y., Wong, T. N., & Nathan, G. K. (2001). Numerical and experimental studies of refrigerant circuitry of evaporator coils. *International Journal of Refrigeration*, *24*(8), 823–833. https://doi.org/10.1016/S0140-7007(00)00050-5

Lifferth, S. O. (2009). *Design and Construction of a New Psychrometric Chamber*. Oklahoma State University.

Myers, R. H., & Montgomery, D. C. (1995). *Response Surface Methodology: Process and Product Optimization Using Designed Experiments*. New York: John Wiley and Sons.

Sarfraz, O., Bach, C. K., & Bradshaw, C. (2019a). A novel technique for computationally efficient consideration of cross-fin conduction in fin-and-tube heat exchanger models. *Submitted for Publication in International Journal of Refrigeration.*

Sarfraz, O., Bach, C. K., & Bradshaw, C. (2019b). Discrete modeling of fin-and-tube heat exchangers with cross-fin conduction functionality. *International Journal of Refrigeration.* Retrieved from https://doi.org/10.1016/j.ijrefrig.2019.05.018

Wang, D., Liu, C., Yu, D., & Chen, J. (2016). Influence factors of flow distribution and a feeder tube compensation method in multi-circuit evaporators. *International Journal of Refrigeration*, *73*, 11–23. https://doi.org/10.1016/j.ijrefrig.2016.09.011